Asymmetric Quadrotor Modeling and State-Space System Identification

Christopher Leshikar, Kameron Eves, Nidhin Ninan and John Valasek {cjlesh, kameroneves, nidhinninan, valasek}@tamu.edu
Vehicle Systems & Control Laboratory
Aerospace Engineering Department
Texas A&M University
College Station, TX, 77843-3141

Abstract—Certain dynamic modes of asymmetric quadrotor configurations are difficult to accurately model analytically. This paper synthesizes an analytical nonlinear parametric state-space model of an asymmetric quadrotor, and verifies it using a non-parametric model calculated from experimentally measured inputs and outputs of the actual vehicle. The offline system identification process produces a discrete-time Linear Time Invariant state-space model using the Observer Kalman Identification algorithm. This model is converted to a continuous time model for comparison to the linearized analytical model. Eigenvlaues, modes, and mode metrics are used to compare the parametric and non-parametric linear models. Results presented in the paper demonstrate that the identified linear model compares well to the linearized analytical model and validates the approach.

I. Introduction

Flight vehicles can be modeled as a linear state-space system describing perturbed motion around a trim point (i.e. an equilibrium condition of the full nonlinear system) as shown in Eq. (1):

$$\dot{\boldsymbol{x}}(t) = A(t)\boldsymbol{x}(t) + B(t)\boldsymbol{u}(t) \tag{1a}$$

$$y(t) = C(t)x(t) + D(t)u(t)$$
(1b)

Here $\boldsymbol{x} \in \mathbb{R}^n$ is the perturbed state vector, $\boldsymbol{u} \in \mathbb{R}^m$ is a perturbed control vector, and $\boldsymbol{y} \in \mathbb{R}^p$ is the perturbed output vector. The state matrix $A \in R^{n \times n}$, control influence matrix $B \in \mathbb{R}^{n \times m}$, output matrix $C \in \mathbb{R}^{p \times n}$, and carrythrough matrix $D \in \mathbb{R}^{p \times m}$ describe the system. If the 4-tuple (A, B, C, D) is independent of time it is a Linear Time Invariant (LTI) system.

Flight models are traditionally generated by several methods of varying complexity and fidelity. At the low-fidelity end and for preliminary design [1], linear parametric models of an aircraft can be obtained using linear aerodynamics and empirical techniques [2] with errors in the 10-20% range for the most critical parameters. Aerodynamic prediction codes are then generally used to populate aerodynamics databases over the range of the flight envelope [3], [4]. Wind tunnel tests are then used for verification and validation of the computational models. Finally, models can be obtained from experimental flight data. This is generally the most accurate and the most expensive approach.

Several classes of algorithms exist for generating models of systems from experimental data. Common system identification algorithms include the Eigensystem Realization Algorithm (ERA) [5], Observer/Kalman Identification (OKID) [6], the Comprehensive Identification from Frequency Responses (CIFER®) algorithm [7], Free Response Functions [8], and Observer/Controller Identification (OCID) [9]. Reference [10] provides a historical overview of system identification approaches for flight vehicles. The authors used OKID for system identification in previous works [11]–[13], and subsequently developed and used a commercial-off-the-self (COTS) low size, weight, power and cost (SWaP-C) Developmental Flight Test Instrumentation (DFTI) system[14]. Its high-frequency sampling capability, at a maximum of 100 Hz, makes it ideal for system identification and modeling applications.

This paper develops a method to synthesize and then verify an analytical nonlinear parametric state-space model of an asymmetric quadrotor Unmanned Air Systems (UAS). The model is verified using a non-parametric model synthesized from measured inputs and outputs from flight logs of the actual vehicle. An offline system identification process is conducted using the OKID algorithm, which produces a linear discrete-time state-space model. This model is then converted to a continuous time model for comparison to the linearized analytical model.

II. ASYMMETRIC QUADROTOR STATE-SPACE MODELING

For this work the Newton-Euler formalism and the Euler angles theories are used [15] to generate the generic the 6-DOF rigid body equations for the asymmetric quadrotor. The asymmetric quadrotor was modelled in a cross configuration with M2 and M4 propellers rotating counter-clockwise while M1 and M3 rotating clockwise. Fig. 1 shows the motor configuration and propeller rotational directions.

A. Quadrotor Kinematics

The derivation of the asymmetric quadrotor dynamics is performed in the North-East-Down (NED) inertial and body fixed coordinates. $\{e_N, e_E, e_D\}$ and $\{x_B, y_B, z_B\}$ denote the unit vectors along the respective NED and body frame axis.

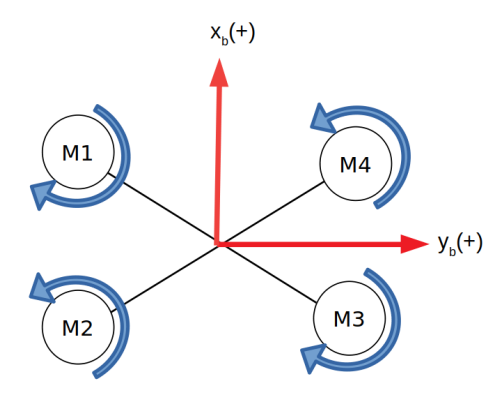


Fig. 1: Motor Rotation and Body Axis

The kinematics of a generic 6-DOF rigid body is defined using Eqn 2.

$$\dot{\xi} = J_{\Theta} \nu \tag{2}$$

where ξ and ν are the generalized velocity vectors with respect to the inertial and body frame respectively;

$$\xi = [\Gamma \quad \Theta]^T = [X \quad Y \quad Z \quad \phi \quad \theta \quad \psi]^T \tag{3}$$

v is composed of linear and angular velocities of the quadrotor as seen in Eqn 4.

$$v = \begin{bmatrix} V & \omega \end{bmatrix}^T = \begin{bmatrix} u & v & w & p & q & r \end{bmatrix}^T \tag{4}$$

 J_{Θ} is the generalized transformation matrix composed of 4 sub-matrix that transforms the linear and rotational elements from body frame to NED Frame.

$$J_{\Theta} = \begin{bmatrix} R_{\theta} & 0_{3\times3} \\ 0_{3\times3} & T_{\theta} \end{bmatrix} \tag{5}$$

The zero sub-matrix fills all the zeros in the matrix expansion while R_{Θ} and T_{Θ} are defined according to the equations

$$R_{\Theta} = \begin{bmatrix} c_{\psi}c_{\theta} & -s_{\psi}c_{\phi} + c_{\psi}s_{\theta}s_{\phi} & s_{\psi}s_{\phi} + c_{\psi}s_{\theta}c_{\phi} \\ s_{\psi}c_{\theta} & c_{\psi}c_{\phi} + s_{\psi}s_{\theta}s_{\phi} & -c_{\psi}s_{\phi} + s_{\psi}s_{\theta}c_{\phi} \\ -s_{\theta} & c_{\theta}s_{\phi} & c_{\theta}c_{\phi} \end{bmatrix}$$
(6)
$$T_{\Theta} = \begin{bmatrix} 1 & s_{\phi}t_{\theta} & c_{\phi}t_{\theta} \\ 0 & c_{\phi} & -s_{\phi} \\ 0 & s_{\phi}/c_{\theta} & c_{\phi}/c_{\theta} \end{bmatrix}$$
(7)

$$T_{\Theta} = \begin{bmatrix} 1 & s_{\phi}t_{\theta} & c_{\phi}t_{\theta} \\ 0 & c_{\phi} & -s_{\phi} \\ 0 & s_{\phi}/c_{\theta} & c_{\phi}/c_{\theta} \end{bmatrix}$$
 (7)

B. Force and Moment.

Gravity and thrust are the two main forces acting on the quadrotor. Other forces like rotor drag, air friction and drag are neglected for this particular asymmetric quadrotor dynamic model. The dynamics of the quadrotor due to the forces and moments acting on the body can be represented as Eqn 8. For preliminary dynamic modelling, the effects due to crosswind and propeller drag are neglected since these influence are often smaller compared to the thrust generated by the motors. Gyroscopic effects produced by propeller rotation are included in this work.

$$\begin{bmatrix} mI_{3\times3} & 0_{3\times3} \\ 0_{3\times3} & I_{3\times3} \end{bmatrix} \begin{bmatrix} \dot{V} \\ \dot{\omega} \end{bmatrix} + \begin{bmatrix} \omega \times (mV) \\ \omega \times (I\omega) \end{bmatrix} = \begin{bmatrix} F \\ \tau \end{bmatrix}$$
 (8)

$$I = \begin{bmatrix} I_{xx} & 0 & 0 \\ 0 & I_{yy} & 0 \\ 0 & 0 & I_{zz} \end{bmatrix}$$
 (9)

I is symmetric because the radially asymmetric quadrotor has an axially symmetric weight distribution. The impact of gravity in the body frame can be found using Eqn 10.

$$F_{NED}^{B} = R_{\Theta}^{-1} F^{NED} \tag{10}$$

For generating rotor dynamics, it is assumed that the forces and moment due to each motor is proportional to the square of the propeller speed. The thrust and torque are modelled as quadratic equations (Eqn 11, 12) but can also be calculated using higher order polynomials for more accuracy. [16]

$$T_i = -b_i \omega_i^{\ 2} \tag{11}$$

$$\tau_i = d_i \omega_i^2 \tag{12}$$

In this work, the motor coefficients b_i and d_i are calculated using motor data provided by the manufacturer. The quadrotor's total thrust force and motor induced moments, $[T \ L \ M \ N]$, are be seen in Eqn 13.

$$\begin{bmatrix} T \\ L \\ M \\ N \end{bmatrix} = \begin{bmatrix} -b & -b & -b & -b \\ -2bl/\sqrt{5} & 2bl/\sqrt{5} & 2bl/\sqrt{5} & -2bl/\sqrt{5} \\ bl/\sqrt{5} & -bl/\sqrt{5} & -bl/\sqrt{5} & bl/\sqrt{5} \\ d & -d & d & -d \end{bmatrix} \begin{bmatrix} \Omega_1^2 \\ \Omega_2^2 \\ \Omega_3^2 \\ \Omega_4^2 \\ (13) \end{bmatrix}$$

C. Asymmetric Quadrotor Mathematical Model

The asymmetric quadrotor's mathematical model can be generated using Eqn 14.

$$M_B \dot{v} + C_B(v)v = G_B(\xi) + O_B(v)\Omega + E_B\Omega^2 \tag{14}$$

where, M_B , $C_B(\nu)$ and $G_B(\xi)$ are the inertia matrix, Corioliscentripetal acceleration matrix, gyroscopic propeller matrix and gravitational vector respectively [15],

$$M_B = \begin{bmatrix} mI_{3\times3} & 0_{3\times3} \\ 0_{3\times3} & I \end{bmatrix} \tag{15}$$

$$C_B(v) = \begin{bmatrix} 0_{3\times3} & -mS(V^B) \\ 0_{3\times3} & -S(I\omega^B) \end{bmatrix}$$
 (16)

$$G_B(\xi) = \begin{bmatrix} F_{NED}^B \\ 0_{3\times 1} \end{bmatrix} \tag{17}$$

$$O_B(v)\Omega = \begin{bmatrix} 0_{3\times 1} \\ q \\ -p \\ 0 \end{bmatrix} \Omega$$
 (18)

where S(.) is the skew-symmetric operator. By expanding the above matrix equation we get the following non-linear equations of motion for the quadrotor.

$$\dot{u} = -qs_{\theta} + rv - qw \tag{19}$$

$$\dot{v} = gs_{\phi}c_{\theta} - ru + pw \tag{20}$$

$$\dot{w} = (-T/m) + g c_{\phi}c_{\theta} + qu - pv \tag{21}$$

$$\dot{p} = (1/I_{xx})(L + (I_{yy} - I_{zz})qr) + J_{TP}q\Omega$$
 (22)

$$\dot{q} = (1/I_{yy})(M + (I_{zz} - I_{xx})pr) - J_{TP}p\Omega$$
 (23)

$$\dot{r} = (1/I_{zz})(N + (I_{xx} - I_{yy})pq) \tag{24}$$

$$\dot{\phi} = p + ((q\mathbf{s}_{\phi} + rc_{\phi})t_{\theta}) \tag{25}$$

$$\dot{\theta} = qc_{\phi} - rs_{\phi} \tag{26}$$

$$\dot{\varphi} = (qs_{\phi} + rc_{\phi})(1/c_{\theta}) \tag{27}$$

For the purpose of system identification, a state-space model for the asymmetric quadrotor is developed. A linear time invariant state-space model is obtained by linearizing the equations of motion using Jacobian. The linear time invariant state-space model is defined as follows.

$$\dot{\boldsymbol{x}} = A\boldsymbol{x} + B\boldsymbol{u} \tag{28}$$

where;

$$x = \begin{bmatrix} u - u_e & v - v_{trim} & w - w_e & p - p_{trim} & \dots \\ q - q_e & r - r_{trim} & \phi - \phi_{trim} & \theta - \theta_{trim} & \varphi - \varphi_{trim} \end{bmatrix}$$
(29)

$$\dot{x} = \begin{bmatrix} \dot{u} & \dot{v} & \dot{w} & \dot{p} & \dot{q} & \dot{r} & \dot{\phi} & \dot{\theta} & \dot{\varphi} \end{bmatrix} \tag{30}$$

$$u = \begin{bmatrix} \Delta \Omega_1 & \Delta \Omega_2 & \Delta \Omega_3 & \Delta \Omega_4 & \Delta \Omega_5 & \Delta \Omega_6 \end{bmatrix}$$
 (31)

The resulting A and B matrix for the linear time invariant state-space model, evaluated at the hovering state as trim condition are;

D. Subtleties of an Asymmetric Quadrotor

The asymmetric quadrotor is not radially symmetric like most quadrotors. This makes it an interesting system to model with system identification. In many ways, the behavior of an asymmetric quadrotor is no different from a symmetric one. The largest and most intuitive change is that the placement of the motors will change the control effectiveness. A basic understanding of moment arms will make it seem like asymmetric quadrotor should have more roll authority then pitch authority. However, this increased control effectiveness is not seen in the control matrix of the state-space model. This is because the effect is overwhelmed by the associated increase in the mass moment of inertia. Counter intuitively, this aspect of the asymmetry has relatively few interesting effects on the stability or dynamics of the vehicle. Certainly some tuning of the chosen control algorithm could be warranted here, but as was seen during this work, the difference is not so large that the pilot cannot account for it. Beyond, the control authority, the only other major effect of an asymmetric vehicle is that the aerodynamic induced dynamics, discussed in the next section, are more likely to occur.

III. AERODYNAMIC EFFECTS AND MOTIVATION FOR SYSTEM IDENTIFICATION

Most dynamic models of a quadrotor ignore aerodynamic effects except for thrust generated by the propellers. If drag is included it is assumed to be colinear with the center of gravity since many quadrotors are designed to minimize drag and trnaslate at relatively low speeds. Including aerodynamics is useful because it can reveal nonlinear stable and unstable nodes. These effects are possible in all quadrotors but much more common in asymmetric quadrotors because the lift and drag coefficients can vary between sides. Stable and unstable aerodynamic nodes are introduced when the vehicle's center of gravity is not axially aligned with the drag. Similar effects can be considered for lift but with the notable exception of vertical takeoff and landing (VTOL) aircraft, these effects are even less important then drag. An asymmetric quadrotor is considered here but the principles are generally applicable. Two different configurations of asymmetric drag are considered. The first is variation along the horizontal plane (x or y axis) the second is variation along the z-axis.

1) Horizontal Drag Offset: A yawing moment is induced when the center of gravity is horizontally offset from the drag axis. In a fixed wing aircraft this is desired and known as weathercock stability, denoted by the stability derivative $C_{N_{\beta}}$. On a quadrotor weathercock stability is usually caused by components that are shielded from the wind in certain orientations or components that have drag coefficients that vary with orientation. If these components are offset from the center of gravity then $C_{N_{\beta}}$ is also found to vary with the vehicle's orientation. As an example, consider a vehicle shaped like the letter H when viewed from above (Fig. 2). The example vehicles are viewed from the top down. There is a stable node and an unstable node. Blue lines represent wind or the induced torque. The maroon lines form the body of an example vehicle with asymmetric drag. Such a vehicle would have increased drag on the side with the cup incident into the wind. However, this effect would be applied axially asymmetrically because the other side would not have the wind incident on the inner face of the cup. This creates a stable node and an unstable node with the vehicle preferentially facing one direction.

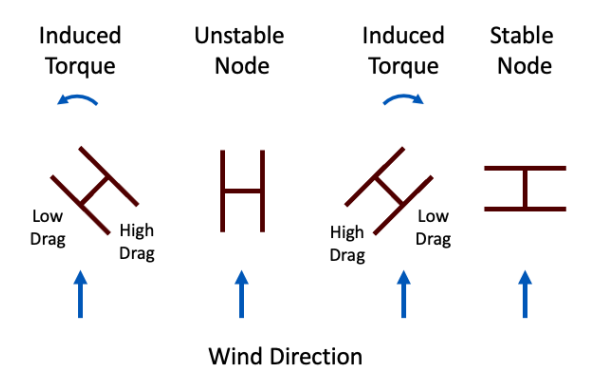


Fig. 2: Effect of Drag on Yawing Moment

- 2) Vertical Drag Offset: In exactly the same way that a torque is induced by a horizontal drag offset, a vertical drag offset also induces a rolling or pitching torque. If the center of gravity (CG) is not aligned with the center of pressure (CP) rotational moments result. The dynamic, and indeed practical, effects of this are notably different from a horizontal offset because the vehicle must pitch or roll to traverse horizontally. This implies that there could be coupling here and even some dynamic modes. Note that only pitching and associated headwind are discussed here without loss of generality. Sideforce and rolling motion follow the same pattern. Figure 3 shows the possible cases. The example vehicles are viewed from the side. Blue lines represent wind or the induced torque. The maroon rectangles form the bodies of an example vehicles. The CP is centered on the windward face
- a) Center of Gravity Below Center of Pressure: When the CG is below the CP the vehicle pitches away from the wind and begins to travel with it. This is a stable mode since the vehicle pitches with the wind and decreases it's velocity relative to the wind. Eventually the vehicle will return to equilibrium and hover relative to the wind. In this new

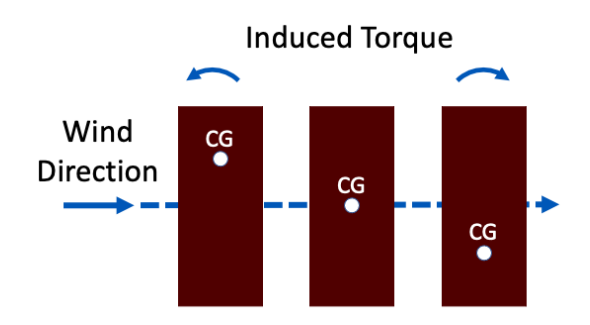


Fig. 3: Effect of Drag on Pitching and Rolling Moment

equilibrium state the vehicle will be translating at the same velocity as the wind. This configuration is desirable if stability is desired.

- b) Center of Gravity Above Center of Pressure: When the CG is above the CP the vehicle pitches into the wind. This is an unstable mode since the vehicle pitches into the wind and increases it's horizontal velocity. If the total thrust is not increased it will accelerate downward. Both of these motions will cause the vehicle to continue its pitching motion and diverge from the hovering equilibrium point. Despite being unstable this configuration can be useful if robustness to wind gusts is desired. The vehicle will accelerate into the wind and, to a certain degree, maintain position relative to the global frame.
- 3) Dihedral: Rotation of the propellors can increase stability. For example, rotating the motors to point toward the center of the vehicle slightly increases stability in the same way that dihedral increases roll stability on a fixed wing aircraft. When the vehicle pitches to traverse horizontally the resultant forward motion will increase the effective Angle-of-Attack (AOA) of the propeller that is upwind, but decrease the effective AOA for the propeller that is downwind. Additionally, the downward motion caused by the rotation of the thrust vector will increase the effective AOA on the upwind propeller. Figure 4 shows that the effective AOA of the propellers causes an increase in thrust on the upwind propeller and a decrease in thrust on the downwind propeller. Theoretically it will also increase the effective AOA of the downwind propeller, but it will do so less than the upwind propeller because of the increased angle. These factors combined result in a restoring force that pushes the vehicle back to a level hover. Quadrotors, which are usually unstable systems, can be made stable in this manner. These concepts are discussed in more depth by Hedayatpour et al. [17].
- 4) Modeling Challenges: Unlike fixed wing aircraft quadrotors are most usefully linearized about a hover flight condition. This removes aerodynamic effects from the linearized models. The instability caused by a rotated lift vector is also lost in this linearization although this result is shared with fixed-wing aircraft. Linearizing about some steady velocity may provide helpful insight, but it is not useful for control synthesis because the model has some inherent direction of flight. This eliminates the advantageous omnidirectional characteris-

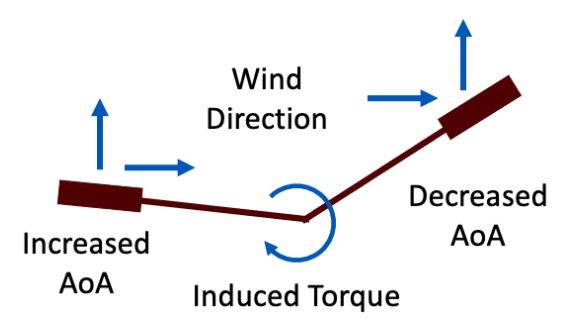


Fig. 4: Quadrotor with Dihedral

tics of a quadrotor. Asymmetric drag is more difficult to model then drag which does not induce a moment. The trigonometric identities and their derivatives that are required for this analysis often involve division by the velocity. Numerical issues are caused by simply setting the velocity to zero. Thus, these terms must be (correctly) dropped when linearizing about hover. Without expensive wind tunnel testing it is difficult to quantify the effect that varying the drag coefficient. Analytical models for this type of behavior do not exist for quadrotors so the analytical model developed in this paper does not include these effects. These deficiencies are intended to be addressed with the identified non-parametric quadrotor model.

IV. OBSERVER/KALMAN FILTER IDENTIFICATION

The Observer/Kalman Filter Identification (OKID) method is a direct Kalman filter gain approach that is formulated in the time-domain and is capable of handling general response data [8]. Because pure impulse excitations are difficult to apply to air vehicles and the noise/signal ratio of sensing data are usually high it is especially valuable for air vehicle modeling. It also allows for nonzero initial conditions and does not require the response to reach steady-state before data collection. OKID was originally developed for elastic spacecraft but has been successfully used to identify state-space models of air vehicles [18], [14]. Because OKID only requires input/output time histories to perform system identification the amount of a priori system specific information is reduced.

The development of the OKID algorithm here generally follows [18]. Starting with linearized, discrete-time, state-space equations augmented with an observer gain:

$$x(k+1) = \bar{A}x(k) + \bar{B}v(k)$$

$$y(k) = Cx(k) + Du(k)$$
(34)

where $\boldsymbol{x}(k) \in \mathbb{R}^n$, $\boldsymbol{y}(k) \in \mathbb{R}^m$, $\boldsymbol{u}(k) \in \mathbb{R}^r$, are state, output and control inputs with

$$\bar{A} = A + GC
\bar{B} = [B + GD, -G]
\mathbf{v}(k) = \begin{bmatrix} \mathbf{u}(k) \\ \mathbf{y}(k) \end{bmatrix}$$
(35)

and $G \in \mathbb{R}^{n \times m}$ is an arbitrary matrix chosen to make the matrix \bar{A} stable. Assuming zero initial conditions and

integer p satisfying $CA^kB\approx 0$ for $k\geqslant p$, substituting and iterating through each time step using Equation (34), the Observer Markov Parameters (OMP) comprised of a input-output relationship becomes

$$\bar{\boldsymbol{y}} = C\bar{A}^p \boldsymbol{x} + \bar{Y}\bar{V} \tag{36}$$

where

$$\bar{y} = \begin{bmatrix} \mathbf{y}(p) & \mathbf{y}(p+1) & \cdots & \mathbf{y}(l-1) \end{bmatrix} \\
\bar{Y} = \begin{bmatrix} D & C\bar{B} & C\bar{A}\bar{B} & \cdots & C\bar{A}^{(p-1)}\bar{B} \end{bmatrix} \\
\bar{V} = \begin{bmatrix} \mathbf{u}(p) & \mathbf{u}(p+1) & \cdots & \mathbf{u}(l-1) \\ \mathbf{v}(p-1) & \mathbf{v}(p) & \cdots & \mathbf{v}(l-2) \\ \mathbf{v}(p-2) & \mathbf{v}(p-1) & \cdots & \mathbf{v}(l-3) \\ \vdots & \ddots & \ddots & \vdots \\ \mathbf{v}(0) & \mathbf{v}(1) & \cdots & \mathbf{v}(l-p-1) \end{bmatrix}$$
(37)

The matrix \bar{Y} is partitioned with the system Markov parameters such that

$$\bar{Y} = \begin{bmatrix} D \ C\bar{B} \ C\bar{A}\bar{B} \ \cdots \ C\bar{A}^{(p-1)}\bar{B} \end{bmatrix} = \begin{bmatrix} Y_0 \ Y_1 \ Y_2 \ \cdots Y_p \end{bmatrix}$$
(38)

from which the OMP are obtained.

$$\bar{Y}_{0} = D$$

$$\bar{Y}_{k} = C\bar{A}^{(k-1)}\bar{B}$$

$$= \left[C(A+GC)^{(k-1)}(B+GD) - C(A+GC)^{(k-1)}G\right]$$

$$= \left[\bar{Y}_{k}^{(1)} - \bar{Y}_{k}^{(2)}\right] \quad k = 1, 2, 3, ...$$
(39)

The general relationship between the actual system Markov parameters and the OMP can be shown to be

$$D = Y_0 = \bar{Y}_0$$

$$Y_k = Y_k^{(1)} - \sum_{i=1}^k \bar{Y}_i^{(2)} Y_{(k-i)} \quad \text{for } k = 1, \dots, p$$

$$Y_k = -\sum_{i=1}^p \bar{Y}_i^{(2)} Y_{(k-i)} \quad \text{for } k = p+1, \dots, \infty$$

$$(40)$$

The next step is to use a singular value decomposition (SVD) on the Hankel matrix:

$$H(k-1) = \begin{bmatrix} Y_k & Y_{k+1} & \cdots & Y_{k+\beta-1} \\ Y_{k+1} & Y_{k+2} & \cdots & Y_{k+\beta} \\ \vdots & \vdots & \ddots & \vdots \\ Y_{k+\alpha-1} & Y_{k+\alpha} & \cdots & Y_{k+\alpha+\beta-2} \end{bmatrix}$$
(41)
$$H(0) = P_n \Sigma Q_n^{\mathsf{T}}$$

The ERA is then used to solve the Hankel matrix for the desired state-space realization (A, B, C, D):

$$\hat{A} = \Sigma_n^{-1/2} P_n^{\mathsf{T}} H(1) Q_n \Sigma_n^{-1/2} \\ \hat{B} = \Sigma_n^{1/2} Q_n^{\mathsf{T}} \\ \hat{C} = P_n \Sigma_n^{1/2} \\ \hat{D} = Y_0$$
(42)

Note that \hat{A} , \hat{B} , and \hat{C} are the estimated system matrices determined using OKID. The $(\hat{A},\hat{B},\hat{C},\hat{D})$ represent the identified discrete linear state-space system:

$$\mathbf{x}(k+1) = \hat{A}\mathbf{x}(k) + \hat{B}\mathbf{u}(k)$$
$$\mathbf{y}(k) = \hat{C}\mathbf{x}(k) + \hat{D}\mathbf{u}(k)$$
 (43)

V. FLIGHT INSTRUMENTATION SYSTEM

Several systems are developed to allow for in-flight dynamic mode excitation and data collection.

A. Airframe Description

The system under test is a modified commercial off-the-shelf (COTS) flight article derived from the Da-Jiang Innovations (DJI) F450 vehicle [19]. The body of the F450 is replaced with long ridged members making the vehicle axially asymmetric. Holes are drilled in these long rigid beams to decrease the weight. Figure 5 shows this modified vehicle, and Table I displays pertinent performance parameters.

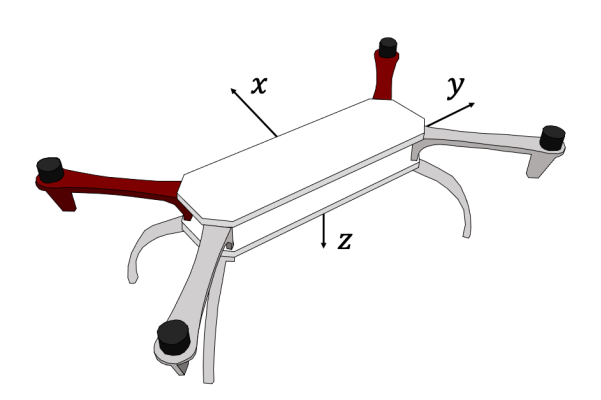


Fig. 5: Modified DJI F450 External Physical Characteristics

TABLE I: Parameters of the Asymmetric Quadrotor Including the Mass of Payload and Batteries

Parameter	Value
Dimensions	28x63x23 cm
Mass	2.5 kg
Mass Moment of Inertia - I_{xx}	54.7 $kg * m^2$
Mass Moment of Inertia - I_{yy}	15.6 $kg * m^2$
Mass Moment of Inertia - I_{zz}	57.2 $kg * m^2$
Cross Moments of Inertia	$0 \ kg * m^2$

The mass moments of inertia are experimentally determined using the compound pendulum technique described in [20]. An image of this experiment in progress is shown in Fig. 6. Note that the vehicle is not radially symmetric, but is axially symmetric so the cross moments of inertia are zero.



Fig. 6: Measuring the Mass Moment of Inertia of the Asymmetric Quadrotor

The motors and propellers are COTS that come standard with the DJI F450. Parameters for the motors and propellers are displayed in Table II.

TABLE II: Parameters of the Motors and Propellers

Parameter	Value
Propeller Size	10x45
Propeller Thrust Coefficient - b	1.6e-5 $N/(rad/s)^2$
Propeller Torque Coefficient - d	1.7e-6 $N * m/(rad/s)^2$
Propeller Mass Moment of Inertia	1.8e-5 $kg * m^2$
Motor Velocity Constant - K_V	960 RPM/V

Equations for the dimensional propeller thrust and torque coefficients can be found by manipulating the definition of a propeller's non-dimensional thrust and torque coefficients, producing the equations

$$b = C_T \rho D^4$$

$$d = C_Q \rho D^5$$
(44)

where D is the diameter of the propeller, ρ is the air density, and C_T and C_Q are the non-dimensional propeller thrust and torque coefficients respectively. These non-dimensional propeller thrust and torque coefficients were obtained from data contained in [21].

Using the propeller and motor model described in [22] a relationship between commanded throttle setting (δ_{T_i}) and propeller RPM (Ω_i) can be determined. This relationship is used to ensure that the analytical model above matches the identified OKID model. It is easier to δ_{T_i} for each motor, but it is easier to work with an analytical model in terms of motor RPM. Note that in this conversion the internal resistance of the motors is assumed to be negligible and the input voltage is assumed to scale proportionally to the throttle setting. The propeller's mass moment of inertia is obtained by approximating the propeller as a thin rod of length and mass equal to the propeller's. This is a reasonable assumption because the propeller is rotating about its short axis so the unusual shape is negligible.

A model of the asymmetric quadrotor is obtained using the analytical model developed above and the experimentally determined values. This analytical model can then be used as a comparison with the OKID identified model, and is presented in the Appendix.

B. Instrumentation

Since the work done in [14] flight controllers are now able to log measurements at over 100 Hz. This enhanced capability greatly simplifies the system identification data logging process. The system developed and used in the present work is called the Developmental Flight Test Instrumentation Two (DFTI2). The Pixhawk 2.1 Blue Cube by Cube Pilot is selected as the stability augmentation system (SAS), and ArduCopter version 4 is used as the software. The Blue Cube has three redundant MPU9250 IMUs each with accelerometers, gyroscopes, and magnetometers, in addition to two redundant barometers. The Blue Cube has vibration isolation to improve the reliability and lifetime of these sensors. The SAS software is running on a STM32F427 Rev 3 Flight Management Unit with a control loop update rate of 500 Hz. This configuration allows for high speed collection of high quality data. The command signal for the motors (i.e. δ_{T_i}) can also be obtained, and the lag between the angular velocities of the motors and the commanded throttle input is assumed to be negligible.

Using USB 2 and the MAVLink protocol the data is streamed to a companion computer and brought to the robot operating system (ROS) using the open source software MAVROS [23]. DFTI2 then serves as a ROS node that subscribes to this published data and writes it to a data file. This allows for a great degree of flexibility as data from heterogeneous sources can easily be logged by publishing the data via a ROS node. This system is also extensible for real-time vehicle system identification. A Jetson Nano running Linux Ubuntu 18.04 and ROS Melodic is used as the companion computer. With a Quad-core ARM A57 CPU running at 1.43 GHz and a 128-core Maxwell GPU, this companion computer has the processing power to sustain high speed data logging. Images of the Flight Controller Unit (FCU) and Jetson Nano computer are shown in Fig. 7.

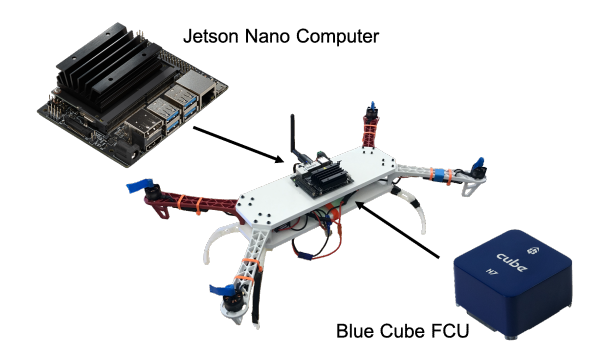


Fig. 7: Locations of the Two Computer Element Before Holes Were Drilled to Save Weight

After completion of the flight the data files are transferred to a laptop or desktop computer where the user can post process the data as needed. While data logging is performed at close to 100 Hz, the post processing serves as a way to assert, via interpolation, that the interval between data points be exactly 0.01 seconds. OKID is then performed using the data sets. Fig. 8 shows an overview of the system architecture and data flow.

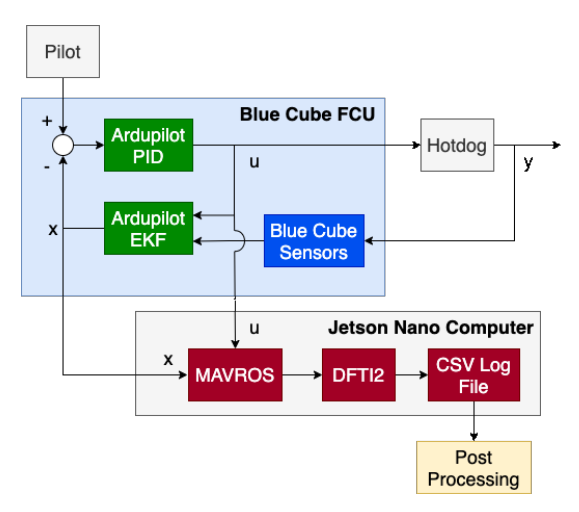


Fig. 8: System Architecture for Data Acquisition

VI. FLIGHT TEST RESULTS

A. Test Plan

Indoor flights are conducted to eliminate exogenous inputs which degrade the overall quality of the data collected. The vehicle is trimmed before each excitation is enjected to improve test data quality.

B. Input Excitation

Automated excitation signals are excite the dynamic modes. Since the modal composition of the asymmetric quadrotor is not known a priori, several types of excitation signals are injected. The excitation signals injected include singlets, doublets, triplets, 3-2-1-1s, and multi-sinusoidal sweeps. One signal type (such as the 3-2-1-1) is injected in a set of three evenly spaced signals so that angular rotation is induced about the inertial x-axis, y-axis, and z-axis. There is no mixing of the signal types when creating the sets, meaning a set such as 2 sine sweep signals paired with a 3-2-1-1 signal (or any other combination of signals) are not injected. The change of magnitude is kept at 10% or less to ensure that dynamics are not driven into the nonlinear range. For the experimental tests the magnitude changes are set to either 5% or 10%. A delay of one second is used between each of the three signals in the set. The periods of singlet signals are set to 0.5 seconds, and the periods of all other signals are set to 1.0 seconds. All of the injected signals are automated by the DFTI2 system. It is found that the 3-2-1-1 signals shown in Fig. 9 produced the best models out of the candidate signal types used.

C. Experimental Results

A total of 100 automated excitation maneuvers are performed and considered for model generation. The maneuvers are performed over 10 flights. A second-order Butterworth filter is applied to the state and control data to remove any noise present in the data. All 100 automated excitation maneuvers that are considered produce unstable models of the vehicle. As a result, the use of plots to compare the time histories of the identified model with the flight data is of little use due to the identified model diverging very quickly as seen in Fig. 11. Therefore other indicators must be used when considering the quality of the model.

The Mode Singular Values (MSV), Modal Controllability Indices (MCI), and Modal Observability Indices (MOI) [24] are used to select the identified modes. These indicators are calculated by

$$MCI = 100 \cdot |B_{\rm m}| \max |B_{\rm m}|$$

$$MOI = 100 \cdot |C_{\rm m}| \max |C_{\rm m}|$$

$$MSV = 100 \cdot \frac{\frac{\sqrt{|B_{\rm m}| \cdot |C_{\rm m}|}}{|1 - |\zeta||}}{\max \frac{\sqrt{|B_{\rm m}| \cdot |C_{\rm m}|}}{|1 - |\zeta||}}$$
(45)

where $B_{\mathrm{m}} \in \mathbb{R}^{nm \times r}$ is the modal input matrix, nm is the number of modes, $C_{\mathrm{m}} \in \mathbb{R}^{m \times nm}$ is the modal output matrix, and $\zeta \in \mathbb{R}^{nm}$ is the eigenvalue vector. These indicators are used to determine the quality of the model. The presence of a SAS on the Blue Cube also presents a challenge in generating a model. With the SAS active during the whole flight, it results in closed-loop dynamics being present. This makes is difficult to determine the open-loop dynamics, which is desired. To minimize the presence of the SAS in the identified model, only flight data from when the automated excitation signal (which overrides the signal from the Blue Cube) is injected.

Comparing the analytical model derived in Section II to the identified model from testing shows that the identified model is close to the derived model, since the time derivatives of the kinematic angles are shown to be primarily a function of the angular rates p, q, r as expected. Note that the sign for qis flipped for θ in A.3. The identified model also identifies the velocities u, v as primarily a function of $q\theta$ and $q\phi$ respectively, with the sign on the θ column element in the p row A.3 being opposite to the analytical model in A.1. Comparing the analytical and identified control influence matrices, the identified B matrix A.4 control derivatives are smaller in magnitude compared to those in the analytical B matrix A.2. The identified modes and characteristics using OKID are shown in Table III where ω_n denotes the natural frequency of second-order modes. The modal indicators of the identified modes are shown in Table IV. The modal composition of the identified model is four second-order modes with one firstorder mode. The identified model is an unstable model, with two of the second-order modes and the first-order mode being unstable.

TABLE III: Identified Modes of the Asymmetric Quadrotor

Mode	Eigenvalue	Damping Ratio	ω_n (rad/s)
1	$0.546 \pm j4.09$	-0.132	4.12
2	$0.515 \pm j2.93$	-0.173	2.97
3	$-1.51 \pm j1.18$	0.789	1.92
4	$-0.172 \pm j0.871$	0.194	0.888
5	0.561	_	0.561

TABLE IV: Modal Indicators of the Identified Modes

Mode	MSV (%)	MCI (%)	MOI (%)
1	67.7	69.1	100.0
2	72.3	100.0	74.3
3	32.5	84.9	51.4
4	100.0	80.3	59.0
5	40.5	42.2	60.2

The use of automated inputs appear to improve the quality of the model identified. Parametric sweeps have not been performed to determine the ideal signal combination for good identification results. Performing parametric sweeps are expected to further improve the results.

VII. CONCLUSIONS

This paper presented the dynamical modeling and verification of an asymmetric quadrotor. Verification of the Linear Time Invariant state-space model was done using offline system identification. Results presented in the paper demonstrate that the 3-2-1-1 input signal contributed to the best identified models, based upon the Mode Singular Values. The Observer/Kalman Filter Identification method correctly predicted the order of the model, based upon all singular values of the identified state matrix being large enough to justify no reduction in model order. The Linear Time Invariant state-space models of the asymmetric quadrotor generated using system identification match the linearized analytical model well in the non-coupling elements. The signs of the control influence matrices match well but the magnitudes do not.

Future work will use the Observer/Controller Identification method to generate an open-loop Linear Time Invariant statespace model. This method will account for the presence of the Stability Augmentation System in the control loop and is expected to improve the identified models. Parametric sweeps of the automated excitation signals will also be performed to determine the signal characteristics that produce the best identified models. Higher quality sensors, in particular a higher quality Inertial Measurement Unit, will be used to obtain more accurate state measurements.

APPENDIX MODELS

A. Parametric Model

The full analytical state-space model is shown in equations A.1 and A.2. This model is linearized about its hover state. The state vector used is $\boldsymbol{x} = [u, v, w, p, q, r, \phi, \theta, \psi]^T$ and the control vector is $\boldsymbol{u} = [\delta_{T_1}, \delta_{T_2}, \delta_{T_3}, \delta_{T_4}]^T$ where δ_{T_i} is the commanded throttle of the ith motor as a percentage and

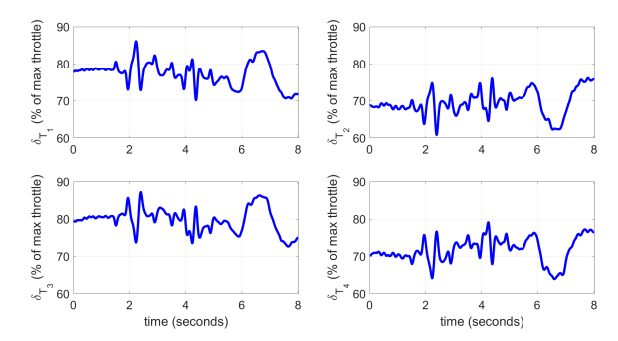


Fig. 9: Control Inputs for the Identified Model

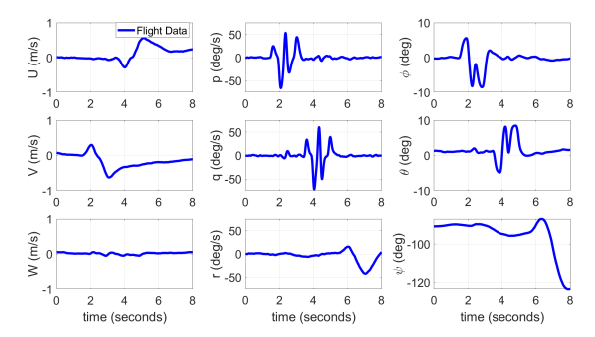


Fig. 10: UAS State Responses to Control Inputs

ranges from 0 to 1. For the trimmed state, $p_1 = q_1 = r_1 = u_1 = v_1 = w_1 = \phi_1 = \theta_1 = 0$, $\delta_{T_i} = 70\%, i = 1, 2, 3, 4$. All units are SI.

B. Identified Model

The full identified state-space model is shown in A.3 and A.4. The state vector used is $\mathbf{x} = [u, v, w, p, q, r, \phi, \theta, \psi]^T$ and the control vector $\mathbf{u} = [\delta_{T_1}, \delta_{T_2}, \delta_{T_3}, \delta_{T_4}]^T$ where δ_{T_i} is the commanded throttle of the ith motor as a percentage ranges from 0 to 1. All units are SI. The identified A matrix is broken

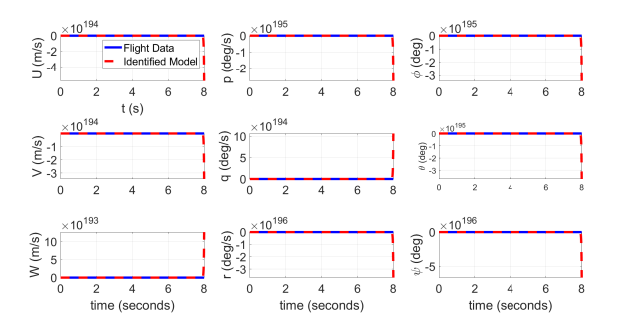


Fig. 11: Comparison of Identified Model and UAS Flight Data

up into the first 5 columns and the last 4 columns for spacing purposes.

$$B = \begin{bmatrix} -0.22 & 3.1 & 2.7 & 0.27 \\ -1.8 & -3.3 & -5.7 & -4.9 \\ -0.66 & -0.20 & -0.46 & 0.63 \\ 52.4 & 31.5 & -45.3 & -27.3 \\ 33.4 & -50.7 & -43.1 & 43.5 \\ -4.8 & 5.3 & -4.8 & 4.9 \\ 0.91 & -0.86 & -6.1 & -4.5 \\ -1.1 & 4.0 & 3.0 & -1.4 \\ -0.50 & 0.75 & -0.79 & 0.80 \end{bmatrix}$$
(A.4)

REFERENCES

- [1] J. Roskam, Airplane Flight Dynamics & Automatic Flight Controls: Part I. DARCorporation, Jan. 2001.
- [2] R. D. Finck et al., "USAF Stability and Control DATCOM," Flight Dynamics Laboratory, Wright Aeronautical Laboratories, Wright-Patterson AFB, OH, Tech. Rep. AFWAL-TR-83-3048, Apr. 1978. [Online]. Available: http://www.dtic.mil/docs/citations/ADB072483
- [3] A. E. Albright, C. J. Dixon, and M. C. Hegedus, "Modification and Validation of Conceptual Design Aerodynamic Prediction Method HASC95 With VTXCHN," NASA Langley Research Center, Tech. Rep. NASA Contractor Report 4712, Mar. 1996. [Online]. Available: https://ntrs.nasa.gov/search.jsp?R=19960022946
- [4] J. Player and D. R. Gingras, "Rapid Simulation Development for Evaluation of Conceptual Unmanned Aerial Vehicles," in AIAA Modeling and Simulation Technologies Conference and Exhibit. Providence, RI: AIAA, Aug. 2004, doi:10.2514/6.2004-5042.
- [5] J.-N. Juang and R. S. Pappa, "An eigensystem realization algorithm for modal parameter identification and modal reduction," *Journal of Guidance, Control, and Dynamics*, vol. 8, no. 5, pp. 620–627, 1985. [Online]. Available: http://dx.doi.org/10.2514/3.20031

- [6] J.-N. Juang, M. Phan, L. G. Horta, and R. W. Longman, "Identification of observer/Kalman filter Markov parameters," *Journal of Guidance, Control, and Dynamics*, vol. 16, no. 2, pp. 320–329, 1993. [Online]. Available: http://dx.doi.org/10.2514/3.21006
- [7] M. B. Tischler and M. G. Cauffman, "Frequency-Response Method for Rotorcraft System Identification: Flight Applications to BO-105 Coupled Rotor/Fuselage Dynamics," *Journal of the American Helicopter Society*, vol. 37, no. 3, pp. 3–17, 1992.
- [8] J.-N. Juang, Applied System Identification. Upper Saddle River, NJ: Prentice Hall, 1994.
- [9] J.-N. Juang and M. Phan, "Identification of System, Observer, and Controller from Closed-loop Experimental Data," *Journal of Guidance, Control, and Dynamics*, vol. 17, no. 1, pp. 91–96, 1994. [Online]. Available: http://dx.doi.org/10.2514/3.21163
- [10] P. G. Hamel and R. V. Jategaonkar, "Evolution of Flight Vehicle System Identification," *Journal of Aircraft*, vol. 33, no. 1, pp. 9–28, 1996. [Online]. Available: http://dx.doi.org/10.2514/3.46898
- [11] T. Woodbury, J. Valasek, and F. Arthurs, "Flight test results of Observer/Kalman Filter Identification of the Pegasus unmanned vehicle," ser. AIAA Paper 2015-1481. Kissimmee, FL: AIAA Atmospheric Flight Mechanics Conference, Jan. 2015.
- [12] F. Arthurs, J. Valasek, and M. D. Zeigler, "Precision Onboard Small Sensor System for Unmanned Air Vehicle Testing and Control," in AIAA Guidance, Navigation, and Control Conference, San Diego, CA, 2016, AIAA Paper 2016-1138. [Online]. Available: http://dx.doi.org/10.2514/6.2016-1138
- [13] J. Harris, J. Henrickson, F. Arthurs, and J. Valasek, "Aircraft System Identification using Artificial Neural Networks with Flight Test Data," in 2016 International Conference on Unmanned Aircraft Systems (ICUAS'16). Arlington, VA: IEEE, Jun. 2016, doi:10.1109/ICUAS.2016.7502624.
- [14] H. Lu, J. Harris, V. G. Goecks, E. Bowden, and J. Valasek, "Flight test instrumentation system for small uas system identification," in 2017 International Conference on Unmanned Aircraft Systems (ICUAS), 2017, pp. 1696–1705.
- [15] T. Bresciani, "Modelling, identification and control of a quadrotor helicopter," Master's thesis, Lund University, 2008.
- [16] A. R. Kim, P. Vivekanandan, P. Mcnamee, I. Sheppard, A. Blevins, and A. Sizemore, "Dynamic Modeling and Simulation of A Quadcopter with Motor Dynamics," 2017. [Online]. Available: http://arc.aiaa.org
- [17] M. Hedayatpour, M. Mehrandezh, and F. Janabi-Sharifi, "A unified approach to configuration-based dynamic analysis of quadcopters for optimal stability," in 2017 IEEE/RSJ International Conference on Intelligent Robots and Systems (IROS), 2017, pp. 5116–5121.
- [18] J. Valasek and W. Chen, "Observer/Kalman Filter Identification for Online System Identification of Aircraft," *Journal of Guidance, Control, and Dynamics*, vol. 26, no. 2, pp. 347–353, 2003. [Online]. Available: http://dx.doi.org/10.2514/2.5052
- [19] D.-J. I. (DJI), FlameWheel 450 User Manual, Da-Jiang Innovations (DJI).
- [20] W. Gracey, "The Experimental Determination of the Moments of Inertia of Airplanes by a Simplified Compound-Pendulum Method," Langley Memorial Aeronautical Laboratory, NASA TN D-1629, 1948. [Online]. Available: https://apps.dtic.mil/dtic/tr/fulltext/u2/a381475.pdf
- [21] G. A. O. D. J.B. Brandt, R.W. Deters and M. Selig, "UIUC Propeller Database," University of Illinois at Urbana-Champaign, Database Vols 1-3, 2020. [Online]. Available: https://m-selig.ae.illinois.edu/props/ propDB.html
- [22] A. Ning, Flight Vehicle Design. self-published, 2018.
- [23] "Mavros package summary," ROS.org, 2018. [Online]. Available: http://wiki.ros.org/mavros
- [24] R. Longman, M. Bergmann, and J.-N. Juang, "Variance and bias confidence criteria for ERA modal parameter identification," in *Astro-dynamics Conference*, 1988, p. 4312.